V International Conference on Computational Methods for Coupled Problems in Science and Engineering
COUPLED PROBLEMS 2013
S. Idelsohn, M. Papadrakakis and B. Schrefler (Eds)

THERMO-CHEMICAL MODELING OF FIBER-POLYMER COMPOSITES IN FIRE FOR FLUID/STRUCTURE INTERACTION

V. BIASI*, G. LEPLAT* AND F. FEYEL†

*ONERA - The French Aerospace Lab
F-31055 Toulouse, France
e-mail: valentin.biasi@onera.fr, web page: http://www.onera.fr/

†ONERA - The French Aerospace Lab
F-92322 Châtillon, FRANCE

Key words: Composite materials, Multiphysics Problems, Fire, Pyrolysis, Homogenization

Abstract. Fiber-polymer composite laminates decompose by pyrolysis or oxidation when submitted to high thermal fluxes. The phenomena of heat and mass transfer occuring in these materials are investigated for 2D geometries. A multi-components approach is used to determine the effective properties of those decomposing materials, depending on component fractions and temperature. The gas flow resulting from degradation reactions is driven by Darcy's law. The degradation of a glass fiber - phenolic resin composite disc exposed to a steady gaussian laser beam is evaluated.

1 INTRODUCTION

Composite materials are being used at an increasing rate in aeronautical structures. Their high tenacity, lightweight and corrosion resistance make those materials appropriate in such applications. However their low durability to fire remains one of the major issues restricting their use. Understanding the decomposition of composite materials submitted to fire, with the support of relevant numerical models, will improve the design of composite structures with respect to safety, environmental and cost reduction constraints.

The degradation of such materials under fire is the result of several combined phenomena. Heat transfers can be considered as the result of conductive effects for limited fluxes (less than $20kW/m^2$) [1]. When thermal fluxes are higher, pyrolysis or oxidation transformations appear and modify the material composition. The effective properties of the composite evolve during the decomposition [2], depending on the temperature and the degradation growth. These transformations produce a solid residue and a gas mixture.

Nomenclature

A	Pre-exponential factor, 1/s
C_P	Heat capacity, J/kg/K
E_A	Activation energy, J/mol
h	Enthalpy, J/kg
k	Thermal conductivity, W/m/K
K	Permeability, m^2
M	Molecular mass, kg/mol
n	Order of reaction
P	Pressure, Pa
Q	Heat reaction per unit mass, J/kg
R	Universal gas constant, J/mol/K
t	Time, s
T	Temperature, K
$\boldsymbol{v}_g$	Averaged gas velocity, m/s
Y	Mass fraction

Greek symbols

α	Absorptivity
ε	Emissivity
φ	Volume fraction
μ	Dynamic viscosity, kg/m/s
ν	Stoichiometric mass coefficient
ρ	Density, kg/m^3
$\dot{\omega}$	Reaction rate, $kg/m^3/s$

Subscripts

0 - f	Initial state - Final state
c - v	Char - Virgin
g - s	Gas - Solid
i - J	Component - Nb. of components
j - J	Gas component - Nb. of gas components
m - M	Reaction - Nb. of reactions

The latter is carried and ejected outside of the material where this gas phase interacts with the surrounding atmosphere (with possibility of ignition), as shown on figure 1.

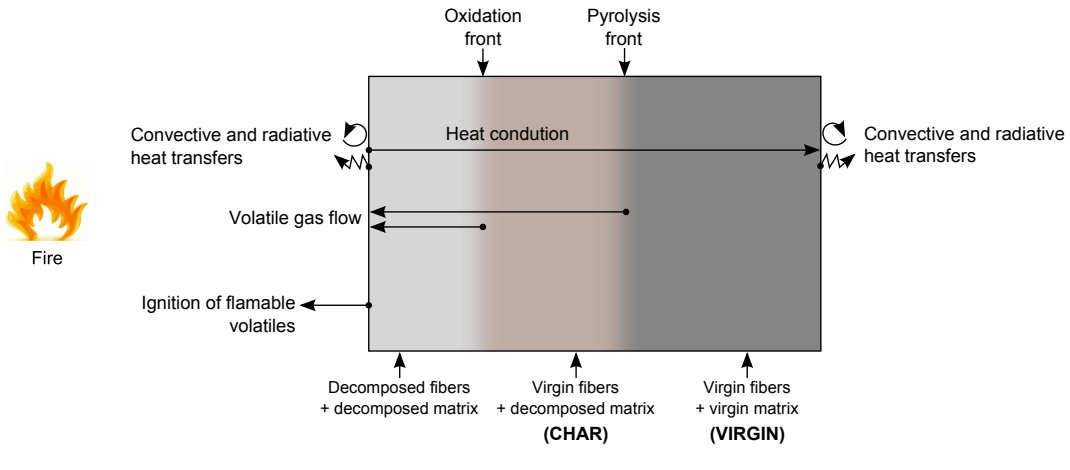

Figure 1: General scheme of the reaction processes in the through-thickness direction of a decomposing composite during fire exposure

Several models have been developed for years to represent the decomposition of composite materials under important heat fluxes, mostly based on Henderson et al. [3, 4]. In these models, a composite in degradation is considered as a mix of virgin and charred material. This approach has been modified and enhanced most notably by Florio et al. [5], Sullivan and Salomon [6, 7], Dimitrienko [8] and Galgano et al. [9]. These studies

bring essential informations about effects of non-thermal equilibrium, thermal expansion or effective stress modifications. Although these models can accurately describe temperature fields within the material, they are limited to 1D cases assuming constant and known heat fluxes.

These assumptions are restrictive for the study of composites in fire because decomposition gases are ejected out of the material and interact with flames. Inflammation of those gases produces an important heat emission [10] which has an impact on thermal flux received by the material, and so on decomposition. Multi-dimensional effects of degradation of composites are rarely investigated [11, 12] although these are essential to take into account fire interactions including accurate heat flux distribution on the impinged surface.

The objective of this work is to propose a model of degradation of composite materials for flame/structure interaction. A major step to achieve this goal is to develop a relevant model which describes thermo-chemical degradation of composite materials under steady heat flux. A bi-dimensional approach is used to model heat and mass transfer in orthotropic materials. The decomposing composite is considered in this model as a multi-components material forming a porous medium. Pyrolysis and oxidation make solid components react to form gaseous mixtures that are transported through the material up to surfaces. Unsteady interface conditions (heat and mass fluxes, gas mixture composition, temperature and pressure) are the input data that will be used to couple the solid decomposition solver with a Navier-Stokes combustion solver.

2 THERMO-CHEMICAL MODELING

The decomposing composite material is represented in this model as a mix of different solid and gas components. Solid components are usually fibers or matrix both at the virgin or charred state, or in a simpler representation the whole solid phase and the charred phase. The gas phase is considered as a mixture of several ideal gases. Throughout this work, a composite material is modeled by a set of I components including J gaseous components. The subscript i is used to refer to any component and the subscript j is used to refer only to a gaseous component.

φ_i and Y_i denote respectively the volume fraction and the mass fraction of each i component. ρ_i denotes the absolute density (mass of i divided by volume of i) and not the bulk density (mass of i divided by total volume, which could be expressed as ρY_i). Absolute density of each solid component is assumed constant ($\rho_i = \rho_{i0}$ if $i \in \{s\}$). The weighted density is given by the relation:

$$\rho = \sum_{i=1}^{I} \rho_i \varphi_i \tag{1}$$

The porosity φ_g is calculated as the volume fraction of the whole gas phase:

$$\varphi_g = \sum_{j=1}^{J} \varphi_j \tag{2}$$

2.1 Properties

The average molecular mass M of the gaseous phase is weighted by gaseous phase volume fractions:

$$M = \frac{1}{\varphi_g} \sum_{j=1}^{J} \varphi_j M_j \tag{3}$$

The surface emissivity ε and absorptivity α are weighted by solid phase volume fractions, which correspond to surface area fractions of each i solid component:

$$\varepsilon = \frac{1}{\varphi_s} \sum_{i=1}^{I-J} \varphi_i \varepsilon_i \quad , \quad \alpha = \frac{1}{\varphi_s} \sum_{i=1}^{I-J} \varphi_i \alpha_i \quad with \quad i \in \{s\} \tag{4}$$

where φ_s is the solid volume fraction. The heat capacity C_P of the material depends on the C_{Pi} of each i component weighted by mass fractions:

$$C_P = \sum_{i=1}^{I} Y_i C_{Pi}(T) \tag{5}$$

and each C_{Pi} depends on temperature using polynomial laws. Sensible enthalpy is calculated, for each component or for the whole material, by integration of heat capacity between the initial temperature T_0 and the current temperature T:

$$h_i = \int_{T_0}^{T} C_{Pi}(\tau) d\tau \qquad and \qquad h = \int_{T_0}^{T} C_P(\tau) d\tau \tag{6}$$

The averaged effective thermal conductivity is defined as a second order tensor. Any j gas component is considered as isotropic ($\overline{\overline{k_j}} = k_j \overline{\overline{I}}$). For every gas or solid component, each coefficient of the associated tensor depends on temperature using a polynomial law. The effective thermal conductivity depends on the fiber diameters and orientations, pore dimensions and distributions, and those particularities should be taken into account. Due to the lack of experimental characterizations, a mixture law (using volume fractions) is used to evaluate $\overline{\overline{k}}$:

$$\overline{\overline{k}} = \sum_{i=1}^{I} \varphi_i \overline{\overline{k_i}} \tag{7}$$

where $\overline{\overline{k_i}}$ is the thermal conductivity tensor of the i component. An ideal gas law is used to calculate the internal pressure as $P = \rho_g \frac{R}{M} T$. Since Reynolds number in these media in

degradation is relatively low [13], the momentum conservation's law can be homogenized using Darcy's law. The latter links the averaged gas velocity vector $\boldsymbol{v}_g$ to the pressure gradient as:

$$\boldsymbol{v}_g = -\frac{K}{\mu_g}\boldsymbol{\nabla} P \tag{8}$$

where μ_g is the gas dynamic viscosity and K the permeability. This value follows a geometric average between the initial value K_0 and the final value K_f:

$$K = K_0^{1-\varphi_g} K_f^{\varphi_g} \tag{9}$$

2.2 Chemical reactions

A set of M chemical reactions is considered to model pyrolysis or oxidation transformations. It is assumed that only solid components can react and that formed gases are inert. The general form of the m reaction is expressed as:

$$\nu_{Rm} R_m \;+\; \nu_{O_2 m}\left(O_2 + \lambda N_2\right) \;\xrightarrow{+Q_m}\; \nu_{Pm} P_m \;+\; \sum_{l=1}^{L}\left(\nu_{ml} G_{ml}\right) \;+\; \nu_{O_2 m}\lambda N_2 \tag{10}$$

where R_m is a solid reactant, $O_2 + \lambda N_2$ is the air (if present and if oxidation reactions occur), P_m is a solid product and G_{ml} is a gas product (in the set of L gas products emitted in the m reaction). ν is used to denote stoichiometric mass coefficients and λ is the mass ratio of N_2 on O_2 in the air, which equals to 3.26.

The heat of reaction Q_m is introduced to express the generated or consumed heat in the m reaction for each consumed quantity of R_m. The reaction rate of R_m is driven by an Arrhenius law:

$$\dot{\omega}_{Rm} = -f(O_2)\left(\rho_R\varphi_R\right)_0 \left(\frac{\rho_R\varphi_R}{\left(\rho_R\varphi_R\right)_0}\right)^{n_m} A_m.exp\left(\frac{-E_{A_m}}{RT}\right) \tag{11}$$

where A_m, E_{A_m} and n_m are the Arrhenius parameters for the m reaction. Terms with the subscript "0" correspond to quantities at the initial state (before that any degradation reaction occurs). The factor $f(O_2)$ in equation 11 allows to take into account the oxygen concentration on the reaction rate $\dot{\omega}_{Rm}$, as:

$$f(O_2) = 1 \; if \; \nu_{O_2 m} = 0, \qquad f(O_2) = \left(\frac{\rho_{O_2}\varphi_{O_2}}{\left(\rho_{O_2}\varphi_{O_2}\right)_0}\right)^{n_{O_2 m}} \; otherwise \tag{12}$$

The reaction rate $\dot{\omega}_{Rm}$ is linked to other $\dot{\omega}_{im}$ reaction rates for each i component which takes part in the m reaction:

$$\dot{\omega}_{im} = \delta_{im}\frac{\nu_{im}}{\nu_{Rm}}\dot{\omega}_{Rm} \tag{13}$$

where δ_{im} sets the sign of the reaction rate in equation 13: $\delta_{im} = +1$ if i is a reactant and $\delta_{im} = -1$ if i is a product in the m reaction. The total source term of the i component (formation and destruction) is the sum of all reaction rates $\dot{\omega}_{im}$ where i takes part in the set of M reactions:

$$\dot{\omega}_i = \sum_{m=1}^{M} \dot{\omega}_{im} \tag{14}$$

Another remarkable value is $(\dot{\omega}_R Q)$, the total heat source produced or consumed by the whole M reactions:

$$(\dot{\omega}_R Q) = \sum_{m=1}^{M} \dot{\omega}_{Rm} Q_m \tag{15}$$

where Q_m is the heat of reaction in m.

2.3 Conservation laws

All conservation laws in this section correspond to averaged local equations. A mass conservation law is written for each i component (solid or gas). The mass variation is caused only by degradation reactions for solid components, considered as a source term.

$$\frac{\partial}{\partial t}\left(\rho_i \varphi_i\right) = \dot{\omega}_i \tag{16}$$

Concerning gas components, mass variations result from gas production or consumption as well as bulk gas transport. This transport term is driven by the pressure gradient as expressed in equation 8. The gas component mass conservation is:

$$\frac{\partial}{\partial t}\left(\rho_j \varphi_j\right) = -\boldsymbol{\nabla} \cdot \left(\frac{Y_j}{Y_g} \rho_g \boldsymbol{v}_g\right) + \dot{\omega}_j \tag{17}$$

This equation is also valid for O_2 if needed. The local thermal equilibrium is assumed in the material, meaning that there are no local temperature difference between all components. Kinetic energy and pressure work are ignored in the energy conservation.

$$\frac{\partial}{\partial t}\left(\rho h\right) = -\boldsymbol{\nabla} \cdot \left(-k \boldsymbol{\nabla} T + h_g \rho_g \boldsymbol{v}_g\right) + \left(\dot{\omega}_R Q\right) \tag{18}$$

In this conservation law, the left hand side represents the internal energy variation for all components. The first right hand side term is the contribution of fluxes. The latter is composed of the conduction term and of the energy transport term of the whole gas phase. The last term is the energy source term, contribution of all heat released for the M reactions. These governing equations are forming a set of $I + 1$ partial differential equations that has to be solved.

3 NUMERICAL METHODS

A numerical solver has been developed for 2D (planar or axisymetric) geometries, using a finite volume numerical method to discretize the equations developed in 16, 17 and 18. Those equations are integrated over small volumes in unstructured meshes, then divergence terms are converted into surface integrals using the divergence theorem. Natural variables (T, P, ρ, φ_i, Y_i) are interpolated at surface centers and all properties developed in section 2.1 are calculated from those natural variables. Gradients are evaluated at cell centers using the gradient theorem from known values at adjacent cells. The integration in time is performed using an implicit theta-scheme. Since Arrhenius based source terms can cause stability problems due to non linearity and slow characteristic times, source terms are integrated explicitly using sub-time steps.

4 RESULTS

4.1 Study case

An evaluation of this bidimensional solver is performed using a glass fiber - phenolic resin composite material, designated as H41N. Material properties were characterized by Henderson et al. [4] and are summarized in table 1. These properties have been established for the virgin and the charred state, and as a consequence three components are used to describe the decomposing composite: "v" the virgin component, "c" the char component and "g" the gaseous phase. Thermal conductivities are arbitrarily modified to illustrate orthotropic heat transfers.

Table 1: Modified properties of H41N (temperatures in Kelvin)

ρ_v	$[kg/m^3]$	2040.6	K_0	$[m^2]$	2.60×10^{-18}
ρ_c	$[kg/m^3]$	1980.7	K_f	$[m^2]$	1.14×10^{-16}
M_g	$[kg/mol]$	18.35×10^{-3}	$\varepsilon_v - \alpha_v$	$[-]$	0.6
k_{v_x}	$[W/m/K]$	$1.12 + 3 \times 10^{-3}T$	$\varepsilon_c - \alpha_c$	$[-]$	0.9
k_{v_y}	$[W/m/K]$	$0.35 + 5 \times 10^{-4}T$	μ_g	$[kg/m/s]$	$8.0 \times 10^{-6} + 2.5 \times 10^{-8}T$
k_{c_x}	$[W/m/K]$	$1.12 + 3 \times 10^{-3}T$	φ_{g0}	$[-]$	0.113
k_{c_y}	$[W/m/K]$	$0.35 + 5 \times 10^{-4}T$	φ_{gf}	$[-]$	0.274
k_g	$[W/m/K]$	$-8.4 \times 10^{-3} + 1.4 \times 10^{-4}T$	Q	$[J/kg]$	-234×10^3
C_{Pv}	$[J/kg/K]$	$791.3 + 1.09T$	A	$[-]$	1.98×10^{29}
C_{Pc}	$[J/kg/K]$	$600.4 + 1.02T$	E_A	$[J/mol]$	2.6×10^5
C_{Pg}	$[J/kg/K]$	$2096 + 1.05T$	n	$[-]$	17.33

The chosen domain is a $80mm$ diameter and $4.16mm$ thick disc. A gaussian laser beam impacts the upper face, centered on the symmetry axis. The computational domain is reduced to an axisymmetric rectangle of $40mm$ along the $\boldsymbol{X}$ axis (representing the disc radius) and $4.16mm$ along the $\boldsymbol{Y}$ axis. This domain is splitted into uniform rectangular cells ($1mm$ along $\boldsymbol{X}$ and $0.208mm$ along $\boldsymbol{Y}$) and the time step is fixed at $0.1s$.

All domain boundaries are considered at atmospheric pressure ($P_0 = 101\ 325Pa$). On surfaces, convective heat transfers are neglected but radiative heat transfers are considered

between surfaces and the surrounding atmosphere temperature (fixed at $293K$). At the initial state, the whole domain is at $T_0 = 293K$ and at atmospheric pressure P_0. The surrounding atmosphere is considered as inert (non-oxidative) and only one reaction drives the degradation (where Arrhenius coefficients E_A, A and n are detailed in table 1). The virgin material "v" pyrolyses to form the char material "c" and gaseous phase "g", with stoichiometric mass coefficients:

$$v \xrightarrow{Q} 0.795\ c + 0.205\ g \tag{19}$$

Between $t = 0s$ and $t = 400s$, a gaussian heat flux is applied on the upper surface, with a maximal intensity of $318.3kW/m^2$ along the symmetry axis and a half-width of $10mm$ at $1/e^2$.

4.2 Discussions

Figure 2 shows a mirror view of the domain at four different times after the degradation begins. Temperature fields are presented on the right hand side and pressure fields on the left hand side of the axis. Averaged gas velocities are represented by vectors only on the domain boundaries. Figure 3 shows temperatures and virgin mass fractions, and figure 4 shows internal pressures extracted along the symmetry axis at the same different times detailed in figure 2.

Temperature is quickly high enough on the front face ($T = 940K$ at $t = 50s$) to cause pyrolysis. As a consequence, the virgin mass fraction on the front face has considerably decreased after $t = 50$ seconds ($Y_v = 0.45$ at $Y = 4.16mm$). The virgin component consumption produces a gaseous phase, and so the internal pressure increases significantly ($P_{max} = 10.4 \times 10^5 Pa$ at $t = 50s$). The formed gases are concentrated around the symmetry axis (see figure 2). The atmospheric pressure imposed at all boundary surfaces produces pressure gradient and as a consequence the gaseous phase flows through the material up to the front face where averaged gaz velocity exceeds $3.2mm/s$ at $t = 50s$ along the symmetry axis (see figure 5).

The pressure peak continues to increase up to $P_{max} = 11.8 \times 10^5 Pa$ at $t = 100s$. It induces important pressure gradients in both directions along the symmetry axis (see figure 4) while decomposition gases ejection remains mainly located at the front face and negligibly at the rear face, as depicted in figures 2 and 5. This difference is explained by higher permeability values in decomposed regions which result in a higher gas velocity even if pressure gradients have the same order of magnitude on both sides.

Then the pressure peak begins to decrease after $100s$ and reaches $9.6 \times 10^5 Pa$ at $t = 200s$. At this time, the degradation reached the rear face as shown by the virgin mass fraction in figure 3 ($Y_v = 0.98$ at $t = 200s$ and $Y = 0mm$). As a consequence, the burnthrough phenomenon causes a release of the gaseous phase with an increasing gas velocity at the rear face until $t = 400s$ and an important decrease of the internal pressure ($P_{max} = 3.6 \times 10^5 Pa$ at $t = 400s$) within the material.

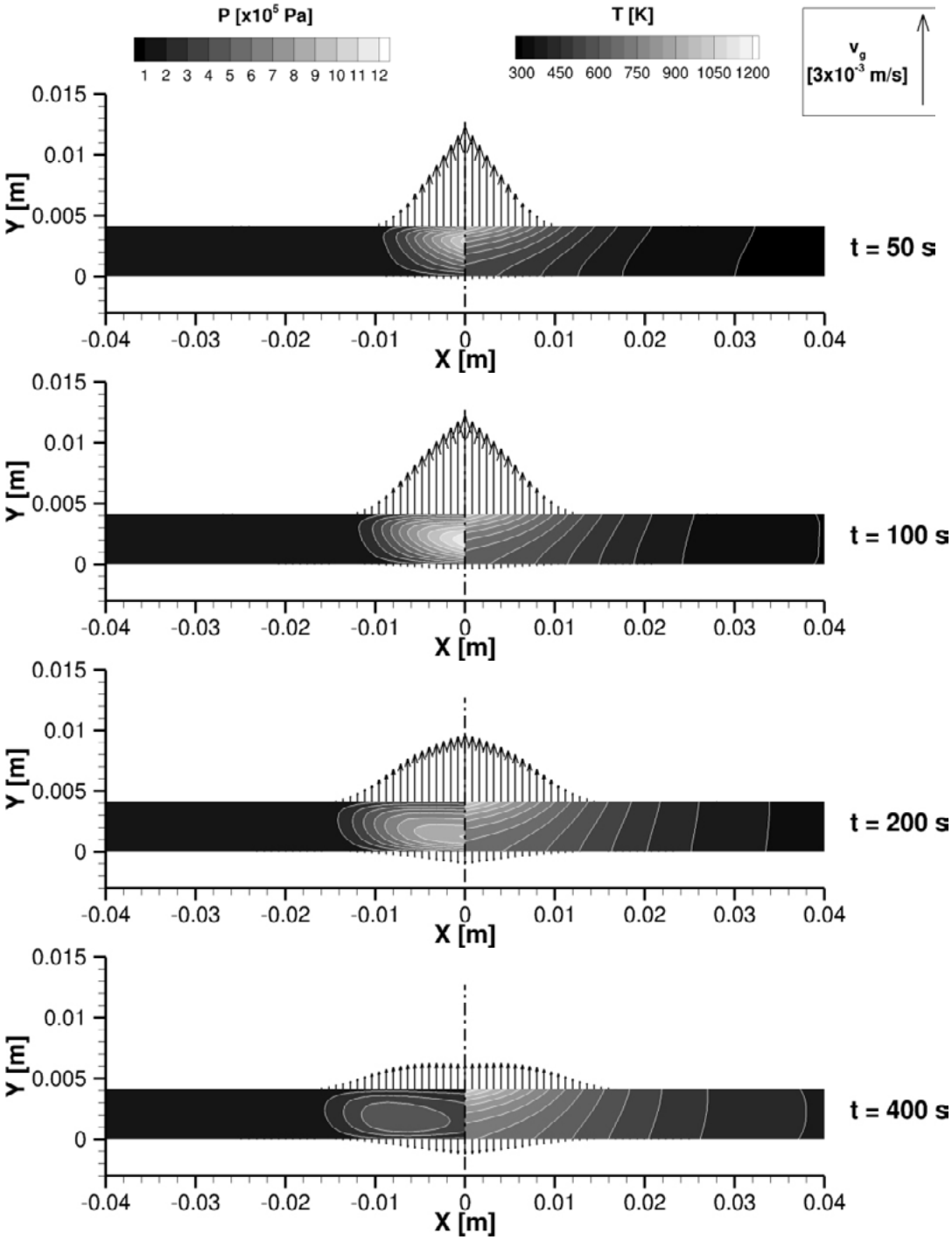

Figure 2: Temperature (right hand side) and pressure (left hand side) distributions associated with averaged gas velocities on surfaces extracted at different times

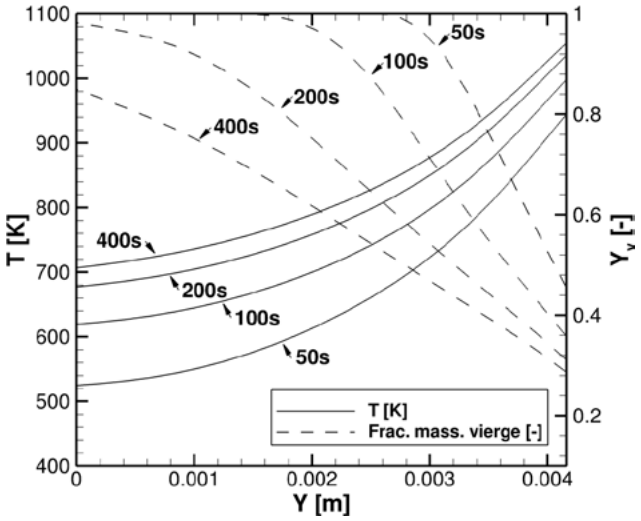

Figure 3: Temperature and virgin mass fraction along tha symmetry axis

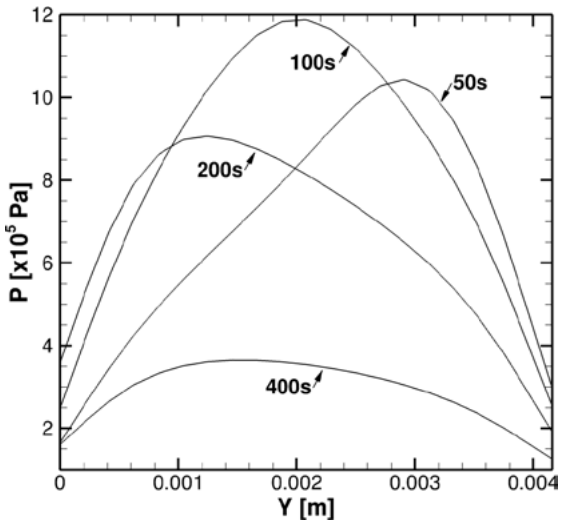

Figure 4: Internal pressure along the symmetry axis

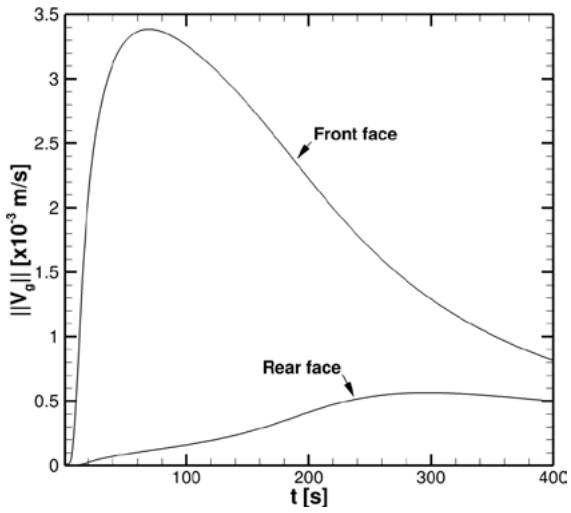

Figure 5: Norm of averaged gas velocity at the front and rear face at $X = 0mm$

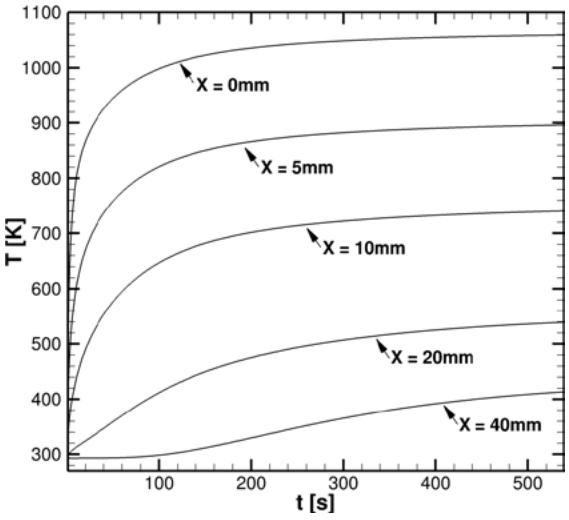

Figure 6: Evolution of temperature on the front face

Afterwards, either on the front or rear faces, the gas outlet profile tends to spread out of the laser beam region (beyond $20mm$ width). The conductive heat transfer, higher along $\boldsymbol{X}$ due to orthotropic conductivities, generates high enough temperature increase to cause pyrolysis in the peripheral region too (see figure 6). Finally, the gaseous phase production does not occur any longer in the symmetry axis region but moves away along the $\boldsymbol{X}$ axis as shown by the pressure peak location over the domain at $t = 400s$ and the associated velocity vectors at the boundaries in figure 2.

5 CONCLUSIONS

A model has been developed with the aim to predict thermo-chemical degradation phenomena on most fiber-polymer composites submitted to non-uniform fluxes. The multi-components formulation, associated with a specific description of each component, allows describing detailed transformations within the material.

An experimental study will be performed to validate the developed model using a configuration similar to the study case developed in section 4 and from the assessment of all material properties. However, the more important the number of components is, the more significant the characterization process will be to determine all needed parameters. It is all the more important since the accuracy of the simulations are subject to experimental uncertainties that must be taken into account in further analyses and comparisons of results.

Neverthless, the present approach integrated into a bidimensional solver turns out to be suitable to represent internal thermo-chemical behaviors and expected boundary conditions of a decomposing anisotropic composite material. The unsteady gas ejection profiles have been identified to provide essential information for the investigation of the interaction between the fire and composite surface including the effects of the heat generated by the ignition of those combustible gases.

REFERENCES

[1] J. Milke and A. Vizzini. Thermal response of fire-exposed composites. *Journal of Composites Technology and Research*, 13:145–151, 1991.

[2] A.P. Mouritz and A.G. Gibson. *Fire Properties of Polymer Composite Materials*. Springer, 2006.

[3] J.B. Henderson, J.A. Wiebelt, and M.R. Tant. A model for the thermal response of polymer composite materials with experimental verification. *Journal of Composite Materials*, 19(6):579–595, 1985.

[4] J.B. Henderson and T.E. Wiecek. A mathematical model to predict the thermal response of decomposing, expanding polymer composites. *Journal of Composite Materials*, 21(4):373–393, January 1987.

[5] J. Florio, J.B. Henderson, F.L. Test, and R. Hariharan. A study of the effects of the assumption of local-thermal equilibrium on the overall thermally-induced response of a decomposing, glass-filled polymer composite. *International Journal of Heat and Mass Transfer*, 34(1):135–147, January 1991.

[6] R.M. Sullivan and N.J. Salamon. A finite element method for the thermochemical decomposition of polymeric materials - 2. carbon phenolic composites. *International Journal of Engineering Science*, 30(4):939–951, April 1993.

[7] R.M. Sullivan and N.J. Salamon. A finite element method for the thermochemical decomposition of polymeric materials - 1. theory. *International Journal of Engineering Science*, 30(4):431–441, April 1992.

[8] Yu.I. Dimitrienko. Thermomechanical behaviour of composite materials and structures under high temperatures: 1. materials. *Composites Part A: Applied Science and Manufacturing*, 28(5):453–461, October 1997.

[9] A. Galgano, C. Di Blasi, C. Branca, and E. Milella. Thermal response to fire of a fibre-reinforced sandwich panel: Model formulation, selection of intrinsic properties and experimental validation. *Polymer Degradation and Stability*, 94(8):1267–1280, August 2009.

[10] A.P. Mouritz, Z. Mathys, and A.G. Gibson. Heat release of polymer composites in fire. *Composites Part A: Applied Science and Manufacturing*, 37(7):1040–1054, July 2006.

[11] C. Luo and P.E. DesJardin. Thermo-mechanical damage modeling of a glass-phenolic composite material. *Composites Science and Technology*, 67(7-8):1475–1488, June 2007.

[12] C. Luo, J. Lua, and P.E. DesJardin. Thermo-mechanical damage modeling of polymer matrix sandwich composites in fire. *Composites Part A: Applied Science and Manufacturing*, -:–, 2012.

[13] N. Puiroux. *Transferts Thermiques et d'Humidité dans les Matériaux Composites Ablatables : Effet des Hétérogénéités*. PhD thesis, Institut National Polytechnique de Toulouse, 2004.